

# High resolution X-ray spectroscopy of the Seyfert 1 Mrk 841: insights on the warm absorber and warm emitter gas

A.L. Longinotti<sup>1,2</sup>, E. Costantini<sup>3</sup>, P.O. Petrucci<sup>4</sup>, C. Boisson<sup>5</sup>, M. Mouchet<sup>5,6</sup>, M. Santos-Lleo<sup>2</sup>, G. Matt<sup>7</sup>, G. Ponti<sup>6</sup>,  
A. C. Gonçalves<sup>5,8</sup>

1 MIT Kavli Institute for Astrophysics and Space Research, 77 Massachusetts Avenue, NE80-6011, Cambridge, MA, 02139, U.S.A.

2 ESAC - European Space Astronomy Centre, P.O. Box 78, 28691 Villanueva de la Cañada, Madrid, Spain

3 SRON National Institute for Space Research, Sorbonnelaan 2, 3584 CA Utrecht, The Netherlands

4 Laboratoire d'Astrophysique, UMR 5571, Université J. Fourier/CNRS, Observatoire de Grenoble BP 53, F-38041 Grenoble cedex 9, France

5 LUTH, UMR 8102, Observatoire de Paris, CNRS, Université Paris Diderot, 5 Place Jules Janssen, 92190 Meudon, France

6 APC, UMR 7164, Université Paris 7 Denis Diderot, 75205 Paris cedex 13, France

7 Dipartimento di Fisica, Università degli Studi Roma Tre, Via della Vasca Navale 84, 00146 Roma, Italy

8 CAAUL, Observatório Astronómico de Lisboa, Tapada da Ajuda, 1349-018 Lisboa, Portugal

Received ...;

## ABSTRACT

**Context.** The Seyfert 1 galaxy Mrk 841 was observed five times between 2001 and 2005 by the XMM-Newton X-ray observatory. The source is well known for showing spectral complexity in the variable iron line and in the soft X-ray excess. This paper reports on the first study of Mrk 841 soft X-ray spectrum at high spectral resolution.

**Aims.** The availability of multiple exposures obtained by the Reflection Grating Spectrometer (RGS) cameras allows a thorough study of the complex absorption and emission spectral features in the soft X-ray band.

**Methods.** The three combined exposures obtained in January 2001 and the two obtained in January and July 2005 were analysed using the SPEX software.

**Results.** We detect a two-phase warm absorber: a medium ionisation component ( $\log \xi \sim 1.5\text{--}2.2 \text{ ergs s cm}^{-1}$ ) is responsible for a deep absorption feature in the Unresolved Transition Array of the Fe M-shell and for several absorption lines in the OVI–VIII band; a higher ionisation phase with  $\log \xi \sim 3 \text{ ergs s cm}^{-1}$  is required to fit absorption in the NeIX–X band. The ionisation state and the column density of the gas present moderate variation from 2001 to 2005 for both phases. The high ionisation component of the warm absorber has no effect in the Fe K band. No significant velocity shift of the absorption lines is measured in the RGS data. Remarkably, the 2005 spectra show emission features consistent with photoionisation in a high density ( $n_e \geq 10^{11} \text{ cm}^{-3}$ ) gas: a prominent OVII line triplet is clearly observed in January 2005 and narrow Radiative Recombination Continua (RRC) of OVII and CVI are observed in both 2005 data sets. A broad Gaussian line around 21.7 Å is also required to fit all the data sets. The derived radial distance for the emission lines seems to suggest that the photoionisation takes place within the optical Broad Line Region of the source.

**Key words.** Galaxies: Seyfert – Galaxies: individual:Mrk 841 – Techniques:spectroscopic

## 1. Introduction

The model that explains Active Galactic Nuclei (AGN) as being powered by accretion on a supermassive black hole surrounded by gas (Rees, 1984), is nowadays generally accepted. In the last decade, the advent of high-resolution X-ray spectroscopy allowed the detailed study of ionised material outflowing along the line of sight within the central region (e.g. Kaspi et al. 2001; Kaastra et al. 2002). Multi-wavelength simultaneous observations have shown that X-ray outflows and UV winds are tightly connected and that the absorption must take place in a material with multiple ionisation layers (Gabel et al. 2005). More than 50% of the Seyfert 1 galaxies are characterised by this gas, which is mostly revealed in the X-ray band through the detection of narrow absorption features from ionised elements, as, for example, Carbon, Oxygen, Neon, Iron (Creenshaw et al. 2003; Blustin et al. 2005).

The structure of the outflowing wind and its relation to the central engine where the AGN continuum radiation is originated,

are not entirely clear. The absorbing gas seems to be diversely distributed in individual sources, its location spanning from a scale of light days in NGC 4051, (Krongold et al. 2007) to few pc in NGC 3783, (Behar et al. 2003).

Variability of the ionised absorbers can often offer a key to study the change in the opacity of the gas in relation to the continuum emission. For example, long Chandra observational campaigns on bright Seyfert Galaxies yielded a variety of results on the response of the warm absorber to the source luminosity fluctuations (Netzer et al. 2002; Krongold et al. 2005).

More recent studies have shown that the presence of emission lines in the soft X-ray band brings additional information on the circumnuclear ionised gas. In some Seyfert 1s, emission lines from highly ionised species can be originated very close to or within the Broad Line Region of the AGN (Costantini et al. 2007; Longinotti et al. 2008), but only in sources with high signal-to-noise it has been possible to relate the X-ray emitter with the X-ray absorber (NGC 3783, Behar et al. 2003).

Mrk 841 is a bright Seyfert 1 galaxy at  $z = 0.0365$  (Véron-Cetty & Véron, 2001) that was observed by several X-ray obser-

**Table 1.** *XMM-Newton* observation log for Mrk 841

Date (yyyy/mm/dd)	OBSID -	Exp (ks)	<sup>1</sup> count rate Cts/s	<sup>2</sup> F <sub>0.3–2keV</sub> (10 <sup>-12</sup> cgs)
2001/01/13	0112910201	10	0.63±0.01	26.6±1.0
2001/01/13	0070740101	12	0.72±0.01	26.6±1.0
2001/01/14	0070740301	14	0.71±0.01	26.6±1.0
2005/01/16	0205340201	45	0.19±0.01	7.5±0.5
2005/07/17	0205340401	30	0.23±0.01	9.1±0.1

<sup>1</sup> In RGS 2<sup>2</sup> Not corrected for absorption; the 2001 flux refers to the global fit of 3 data sets

vatories in the past. Spectral variability was reported in *EXOSAT*, *Ginga* and *ROSAT* data by George et al. (1993), and Nandra et al. (1995). Evidence for a broad iron emission line was found in the *ASCA* spectra reported by Nandra et al. (1997). Weaver, Gelbord & Yaqoob (2001) have reported marginal evidence for variability of the line. The analysis of broad band *BeppoSAX* data revealed the presence of a soft X-ray excess and a Compton reflection component (Bianchi et al. 2001, 2004), although these authors found that warm absorption provided an equally good description of the soft X-ray data. Evidence for a moderately deep OVII absorption edge was also reported in *ASCA* data by Reynolds (1997). *XMM-Newton* data at CCD resolution highlighted the presence of a variable and complex narrow Fe K $\alpha$  line (Petrucchi et al., 2002, Longinotti et al. 2004, Petrucci et al. 2007). Besides the study of Fe K band, the latter paper focuses on the analysis of the soft excess in Mrk 841 by testing two competing models. On one hand, the soft excess can be modeled by reflection off a photoionised accretion disc whose spectrum is relativistically blurred and smeared (Crummy et al. 2006). A valid alternative model was proposed by Gierlinski & Done (2004) who explained the soft excess as arising from ionised absorption in a relativistically smeared wind. According to Petrucci et al. (2007), both models were statistically indistinguishable in the EPIC data of Mrk 841.

The present paper presents the very first analysis of the high-resolution soft X-ray spectra of Mrk 841 and it makes use of all the available *XMM-Newton* data sets, i.e. the five observations previously studied by Petrucci et al. (2007).

## 2. The XMM-Newton Observations

Mrk 841 has been observed by *XMM-Newton* 3 times in 2001 and twice in 2005 (Table 1). In this paper, we present only the high-resolution spectra gathered by the RGS instrument (den Herder et al., 2001). For more details on the EPIC data and on the broadband spectrum, the reader is deferred to Petrucci et al. (2007). All the raw data have been processed with SAS version 7.0.0. Spectral files for source and background were produced by running the standard procedure *rgsproc*. Response matrices have been created by the task *rgsrmfgen*. The observation performed in January 2005 presents an anomaly in the illumination of CCD 2 (for both RGS1 and RGS2). The background subtraction was checked and confirmed to be unaffected by this event.

The source has been varying significantly in flux and spectral shape over the time covered by *XMM-Newton* observations (see Table 1 and see Petrucci et al. 2007 for an extensive discussion on the variability properties of the source). The soft X-ray

flux decreased by a factor of  $\sim 3.5$  from 2001 to 2005, thus it is necessary to consider these two “epochs” separately.

The three short exposures of 2001 have been checked carefully to decide whether the six RGS1 and RGS2 could be combined in two spectra, one for each instrument. We fitted the spectra with the same model to check the agreement in the spectral shape and in the flux level. No significant variation is found in the spectral shape in the RGS band, but since the count rates for the 2001 exposures differ by a few percent (see Table 1), instead of co-adding the data we decided to fit simultaneously the six spectra of 2001 assuming the same fitting model and normalising the data to the RGS1 in observation 0112910201.

This approach is maintained throughout the paper and we will refer to the 2001 simultaneously fitted spectra simply as “Jan 2001”. Since the exposures of 2005 are separated by 6 months, we checked if they could be combined in a single one. After fitting the two 2005 spectra with a power law, the spectral slopes were found to be different by  $\sim 20\%$ , therefore the 2005 spectra were not co-added in the analysis.

In summary, the three epoch spectra will be kept disjointed during the entire spectral analysis and they will be referred to as Jan 2001, Jan 2005 and July 2005.

## 3. RGS Spectral analysis

The spectral analysis of RGS has been carried out by using the latest version of the fitting package SPEX (Kaastra et al. 1996)<sup>1</sup>.

Galactic absorption of column density  $N_H = 2.7 \times 10^{20} \text{ cm}^{-2}$  is included in all the following spectral fits (Dickey & Lockman, 1990). The galactic absorption is modeled with the SPEX HOT component with a temperature fixed to  $5 \times 10^{-4} \text{ keV}$ . For all spectral models, we adopted Solar elemental abundances (Anders & Grevesse, 1989).

The first order spectra have been rebinned of a factor of 3 over the range 7 to 35 Å and the C-statistics is adopted (Cash, 1979). Errors are quoted at the 90% confidence level for one interesting parameter. Throughout the text and tables, the quoted wavelengths are corrected for the cosmological redshift.

### 3.1. The warm absorber

At first glance, the visual inspection of the fluxed spectra (i.e. the spectrum plotted in flux units rather than counts/sec) reveals the typical signatures of absorption from the so-called Unresolved Transition Array of the Fe M shell in the 15–16 Å band (e.g. Sako et al. 2001). The feature appears to be prominent in Jan 2005, but it is easily recognisable also in the other two data sets. We checked the residuals after fitting the spectra with a simple power law, confirming the presence of absorption in all of them, although with different characteristics. This may suggest the occurrence of variability in the ionised material along the three epochs and/or the presence of a multi-component warm absorber. In order to compare the three spectra and test this hypothesis, we have taken the approach to initially fit them with the same model.

We constructed a warm absorber model with the SPEX built-in model XABS. The ionisation balance has been calculated by assuming the Spectral Energy Distribution (SED) of Mrk 841 as the ionising continuum spectrum. The SED was constructed by using the simultaneous Optical-UV-to-X-ray fluxes extracted from the Optical Monitor and the EPIC instruments onboard

<sup>1</sup> See also <http://www.sron.nl/spex>

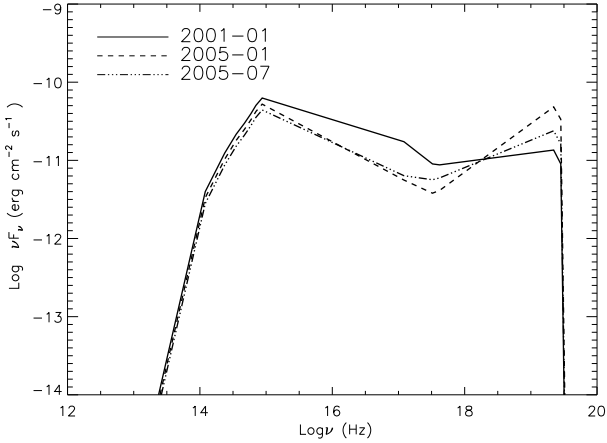


**Fig. 1.** Spectral Energy Distribution of Mrk 841 constructed from the *XMM-Newton* data in the Optical-X-ray band and from the standard AGN radio-IR continuum included in CLOUDY (see text for more details).

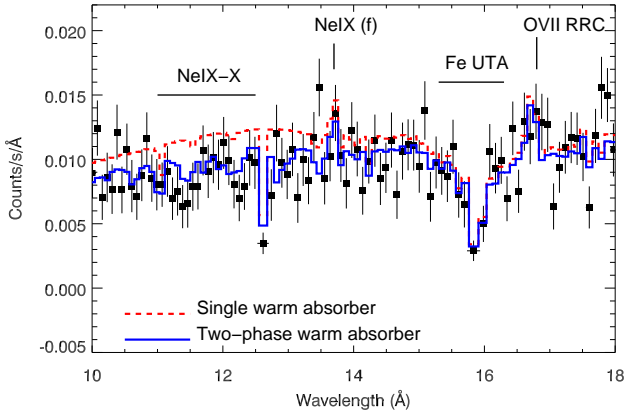


**Fig. 2.** Jan 2005 RGS 2 data modeled with a single component (dashed red line) and a two-component warm absorber (solid blue line). The forbidden emission line of Helium-like Neon and the RRC of OVII, which are included in both models (see Section 3.2), are labelled for clarity.

*XMM-Newton*. For the 2001 data set the photometric point in the U band (centered at 344 nm) has been used. In Jan 2005 and July 2005, the source has been observed with the optical grism which produces a broader band spectrum. For those data sets the flux was extracted at 344 nm. At first approximation the complex X-ray unabsorbed broad band continuum can be modeled as a broken power-law with an energy break at about 1.5 keV (as derived by a phenomenological fit to the EPIC data, see also Fig. 5 of Petrucci et al. 2007). For each of the three data sets, we took the soft power-law index from the RGS and the harder-energies power-law index from Petrucci et al. 2007. The very-low energy portion of the SED (radio to IR) is the same as the standard AGN continuum used in CLOUDY (Ferland et al. 1998). The three SEDs are plotted in Fig. 1.

Then, we constructed a model for the continuum consisting of an underlying single power law absorbed by warm ionised gas and we applied it to the 0.35–1.77 keV data (i.e. the RGS band).

The column density  $N_H$  and the ionisation parameter  $\xi$  of the gas are free parameters. The ionisation parameter is defined as

$\xi = \frac{L}{n_e R^2}$ , where  $L$  is the ionising luminosity in 1–1000 Rydberg,  $n_e$  is the electron density of the gas and  $R$  is the distance of the gas itself from the central source of radiation. The XABS model accounts for the width of the absorption lines through the velocity dispersion parameter. It has been shown in several Seyfert Galaxies that UV and X-ray absorbers originate in the same outflowing gas, thus UV observations can in general provide a reliable limit on the X-ray line broadening (Arav et al. 2007, Costantini et al. 2007). Since no constraint on the velocity dispersion of the UV lines is readily available in the literature on Mrk 841, this parameter has been initially fixed to an average value of 20 km s<sup>-1</sup>. When it is left free in the fitting process, it tends to decrease to zero in all the spectra, thus it has eventually been kept fixed to 20 km s<sup>-1</sup>. Other free parameters in the model are the photon index of the power-law in the RGS band and the outflowing velocity of the warm absorber. The fit statistic improves significantly with the addition of the XABS warm absorber model with respect to the power-law model, but still, the fit is not completely satisfactory for all the three epochs.

A close inspection of the spectra shows that absorption features are visible as negative residuals in the Neon band (12–14 Å). The single warm absorber component is not sufficiently ionised to account for absorption in this band. Therefore, the presence of a second warm absorber with a higher ionisation level was tested by including in the model a second XABS component. The addition of the second warm absorber leads to a fit statistic improvement by  $\Delta C=75$  and  $\Delta C=25$  for 3 d.o.f. measured respectively in Jan and July 2005 spectra. The resulting best fitting parameters are reported in Table 2. The improvement is less significant in Jan 2001, but this is not surprising since the column densities in Table 2 indicate that the absorber may be shallower at this epoch. The effect of the second warm absorber is shown in Figure 2 for Jan 2005: the Fe UTA is clearly well fitted by the medium ionisation phase, whereas the absorption features of NeIX 1s-3p at 11.556 Å and NeX Ly $\alpha$  at 12.132 Å require a more highly ionised plasma to be accounted for.

The two-phase warm absorber provides a good fit to the data as can be seen in Figure 3. The main absorption features are identified with transitions of OVI, OVII, OVIII in the 18–23 Å band, Fe UTA at 15–16 Å and Neon IX-X in the 12–14 Å. No significant velocity shift is detected in any of the two warm absorbers (see Table 2). The upper limits are consistent with outflowing absorbers blueshifted by several  $\times 10^2$  km s<sup>-1</sup>, as commonly observed in Seyfert 1 Galaxies.

Even with the addition of the second warm absorber, the fit of Jan 2005 spectrum is not completely satisfactory, since positive residuals are still present in the OVII band (21–22 Å, see top panel of Figure 4). The analysis of these residuals in emission is reported in the following section.

### 3.2. Emission features in the RGS spectra

#### 3.2.1. Narrow emission lines

We start by fitting Jan 2005 with three narrow line components at the wavelengths corresponding to the rest frame positions of the resonance, intercombination and forbidden lines ( $r$ ;  $i$ ;  $f$ ) in the OVII line triplet at 21.600, 21.790 and 22.101 Å, respectively. The analysis of emission lines in this portion of the spectrum is complex due to the superposition of the absorption lines imprinted by the warm absorber. The peak wavelengths of the three lines are kept frozen to the laboratory values. Since the  $r$  transition has a large oscillator strength in the absorption com-

**Table 2.** Best fitting parameters for the two-phase warm absorber. The soft photon index refers to the power law fitted in the RGS band, i.e. 7-35 Å. The quoted parameters and C-statistic refer to the model including also the emission features in Table 3.

Obs	$\Gamma_{soft}$	$\text{Log}\xi$ (ergs s cm <sup>-1</sup> )	$N_H$ 10 <sup>21</sup> cm <sup>-2</sup>	$v$ km s <sup>-1</sup>	$\text{Log}\xi$ (ergs s cm <sup>-1</sup> )	$N_H$ 10 <sup>21</sup> cm <sup>-2</sup>	$v$ km s <sup>-1</sup>	Cstat/d.o.f.
-	-	-	-	-	-	-	-	-
Jan 01	2.60±0.07	2.2±0.2	1.2±0.5	<1600	3.3 <sup>+0.8</sup> <sub>-0.4</sub>	<17.0	<25000	3082/2725
Jan 05	2.41±0.07	1.5±0.1	2.3±0.5	< 100	3.2±0.1	30.0 <sup>+110</sup> <sub>-20.0</sub>	<100	1958/1435
July 05	2.07±0.07	1.7 <sup>+0.3</sup> <sub>-0.2</sub>	3.9 <sup>+2.6</sup> <sub>-1.6</sub>	<1000	2.8±0.3	7.6 <sup>+18.0</sup> <sub>-5.5</sub>	<1000	1855/1437

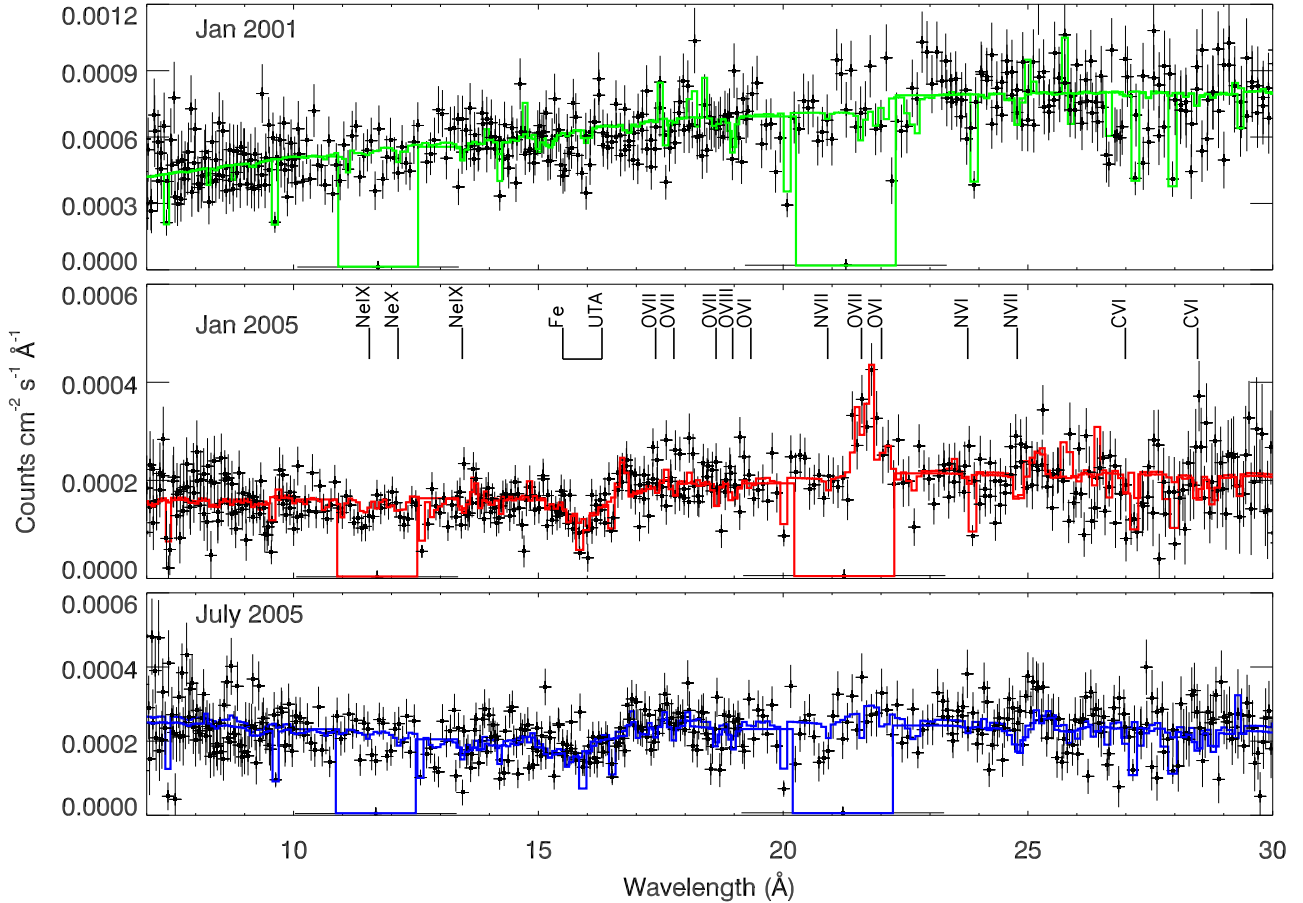


**Fig. 3.** From top to bottom: RGS rest-frame spectra of Jan 2001 (for plotting purpose only obsid 0070740101 is shown), Jan 2005 and July 2005 fitted with the best fit model including the components in Table 2 and 3. For plotting purpose, the spectra are re-binned by a factor of 9 and plotted in the 7-30 Å band, where most of the features of interest fall. The labels mark the ionic species with the highest contribution in our warm absorber model.

ponent, most of the emission line at this wavelength will be re-absorbed, making a precise measure of its flux somewhat difficult. The *i* and *r* components are detected, while only an upper limit is found for the *f* line. Less prominent positive residuals are present in the Neon IX band, hence we searched for emission lines also in this portion of the spectrum. Only the NeIX forbidden component at 13.699 Å is detected (the Neon band is shown in Figure 2). The emission lines fluxes and significances in terms of C statistic improvement for one free parameter, are reported in Table 3. The structure of the line triplet fitted in Jan 2005 data is plotted in Figure 4 (thick red line).

We model the spectra of Jan 2001 and July 2005 with the same emission line components included for Jan 2005. Not surprisingly, giving that the continuum flux is higher in these two

data sets (see Table 1), we could measure only the upper limits on the line fluxes, which are generally consistent with Jan 2005 spectra, except for the OVII resonance line in July 2005 that may be severely underestimated.

### 3.2.2. Radiative Recombination Continua

The spectrum of Jan 2005 displays an additional emission feature around 17 Å, consistent with the position of the Radiative Recombination Continuum (RRC) of OVII (see Figure 2 for a close-up on this feature). A closer look at longer wavelengths suggests that other RRC components from Carbon may give significant contribution in the positive residuals of the data. In our analysis, these features are fitted with the RRC model in SPEX.

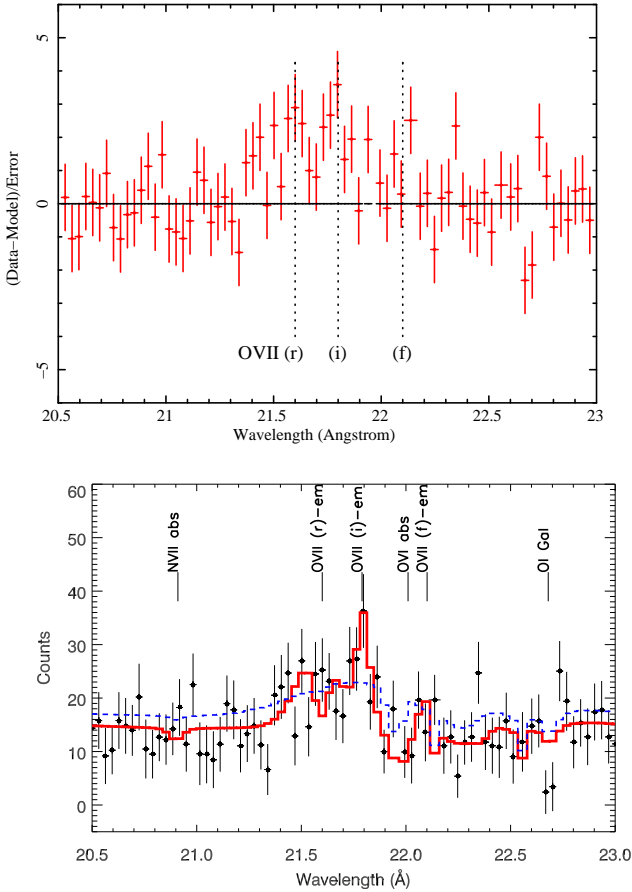


**Fig. 4.** Top: Residuals of the continuum model in the OVII band. Bottom: Zoom on the OVII triplet in Jan 2005. Line parameters are reported in Table 3. The red solid line corresponds to the best fit model (including the emission lines in Table 3 and the underlying warm absorber in Table 2). The blue dashed line shows the underlying OVII broad Gaussian line after removing the contribution of the narrow lines triplet and the warm absorber.

The width of the RRC profiles is a very sensitive indicator of the electron temperature in the recombining plasma (Liedahl & Paerels 1996, Liedahl 1999). Our data suggest the presence of a narrow RRC at the OVII wavelength (see Figure 2), indicative of temperature of  $\text{few} \times 10^4$  K. Therefore, we fit the RRC emission measure<sup>2</sup> of OVII and CVI as free parameters assuming an electron temperature corresponding to  $kT = 3$  eV, i.e.  $T = 3.5 \times 10^4$  K. If the temperature is left free to vary in the fit, we find  $kT = 2.8^{+2.9}_{-1.4}$  eV.

The improvement in the fit statistic for adding the RRC component in Jan 2005 is  $\Delta C = 23$  for 2 degrees of freedom. The OVII RRC seems to be slightly redshifted from its laboratory position; we have applied a small redshift of  $z = 0.001$  to match the observed excess in the data. The same is done for the C VI RRC around 25 Å, where the shift is less evident due to the lower signal-to-noise of our spectra in this band. As described in the previous section for the narrow emission lines, we included the RRC in the model for all the three spectra and we reported the best fitting parameters in Table 3.

<sup>2</sup> The emission measure corresponds to  $n_e n_{\text{ion}} V$ , where  $n_e$  is the gas electron density,  $n_{\text{ion}}$  is the density of the parent ion that recombines to the ground state and  $V$  is the emitting volume

### 3.2.3. Broad Oxygen line

Once the narrow lines are included in the fit, the residuals around the OVII triplet in Jan 2005 still show some structure in excess, particularly on the left side of the resonant line. To account for these residuals, a broad Gaussian line was added in the model with width and wavelength free to vary. The resulting best fitting parameters for this component are  $\lambda = 21.75^{+0.23}_{-0.36}$  Å,  $\text{FWHM} = 0.60^{+0.52}_{-0.35}$  Å and  $\text{flux} = 0.64 \pm 0.53 \times 10^{-4}$  photons  $\text{cm}^{-2} \text{s}^{-1}$ . The addition of the broad line component leads to an improvement of  $\Delta C_{\text{stat}} = 18$  for 3 degrees of freedom, corresponding to a significance level higher than 99%. Figure 4 shows the separate contribution of the Gaussian profile to the best fit model for the OVII line triplet. For simplicity, the broad line at 21.7 Å will be referred to as “OVII line” only, without identifying a specific transition. The same line component was included in July 2005 yielding the following best fit parameters:  $\lambda = 21.71 \pm 0.23$  Å,  $\text{FWHM} = 0.54^{+0.57}_{-0.44}$  Å and  $\text{flux} = 0.51 \pm 0.38 \times 10^{-4}$  photons  $\text{cm}^{-2} \text{s}^{-1}$ . Although the significance of this component in July 2005 (around 90%) is lower than in Jan 2005, the general good agreement in the best fit parameters for the two spectra seem to support the presence of the same line in July 2005. In Jan 2001 data, we added the broad component as we did for the narrow lines. Since the higher continuum flux prevents the determination of the line properties, in order to measure the line flux, the position and width of the Gaussian component have been fixed to the average value found for the 2005 epochs (see Table 3). An upper limit of  $< 0.85$  photons  $\text{m}^{-2} \text{s}^{-1}$  (consistent with the 2005 measurements) was found for the broad component in 2001.

## 4. Discussion

The analysis of the RGS data of Mrk 841 presented herein provides a considerable amount of information. An important contribution from a warm absorber consisting of two ionisation components has been revealed and most interestingly, it proves to be relatively stable on the time scale of 4 years. In addition, the presence of emission features from highly ionised species of Neon, Oxygen and Carbon has been ascertained. These topics will be addressed separately in the following sections. The discussion is based on the results from the global best fit (i.e. absorption+emission), which is reported in Tables 2 and 3.

### 4.1. A two-phase warm absorber in Mrk 841

The properties of the ionised absorber emerging from the spectral fits described in section 3.1, indicate that there are two distinct levels of ionisation in the absorbing gas. A medium phase warm absorber characterised by  $\log \xi$  in the range 1.5–2.2  $\text{ergs s cm}^{-1}$  and column density of the order of  $10^{21} \text{ cm}^{-2}$  is responsible for transition in the Fe UTA and in the Oxygen band.

The availability of spectra from different epochs may allow a variability study of the absorber physical conditions, particularly considering that being the Fe UTA the result of a blend of several charges states, its shape and position are very sensitive to changes in the ionisation balance of the gas and, ultimately, to luminosity variations of the source (Behar et al., 2001). The errors in Table 2 show that  $\xi$  and  $N_H$  are generally consistent through the three data sets, although there seem to be a decrease of ionisation accompanied by a moderate increase of the column density going from 2001 to Jan 2005. Indeed, the Fe UTA is much more evident in both 2005 spectra because the lower ionisation

**Table 3.** Emission lines parameters and emission measure for RRC in the three epochs. For  $\Delta C$  stat  $\leq 3$ , the upper limits on the flux is reported.

Obs -	Line -	$\lambda$ (Å)	Flux ( $10^{-4}$ ph cm $^{-2}$ s $^{-1}$ )	$\Delta C$ -	FWHM (Å)	RRC EM ( $10^{58}$ cm $^{-3}$ )
Jan 01	OVII (r)	21.600	< 0.42	-	0-width	OVII <450 CVI <4300
	OVII (i)	21.790	< 0.15	-	0-width	
	OVII (f)	22.101	< 0.43	-	0-width	
	NeIX (f)	13.699	< 0.12	-	0-width	
	OVII (gau)	21.7	< 0.85	-	0.55	
Jan 05	OVII (r)	21.600	0.24 $\pm$ 0.16	17	-	OVII=1500 $\pm$ 800 CVI=2500 $\pm$ 1800 $\Delta C$ stat=23
	OVII (i)	21.790	0.26 $^{+0.26}_{-0.16}$	16	-	
	OVII (f)	22.101	<0.20	-	-	
	NeIX (f)	13.699	0.10 $\pm$ 0.05	10	-	
	OVII (gau)	21.75 $^{+0.23}_{-0.36}$	0.64 $\pm$ 0.53	18	0.60 $^{+0.52}_{-0.35}$	
July 05	OVII (r)	21.600	<0.04	-	-	OVII=1860 $\pm$ 1000 CVI=2500 $\pm$ 2300 $\Delta C$ stat=15
	OVII (i)	21.790	<0.25	-	-	
	OVII (f)	22.101	<0.23	-	-	
	NeIX (f)	13.699	<0.15	-	-	
	OVII (gau)	21.71 $\pm$ 0.23	0.51 $\pm$ 0.38	6	0.54 $^{+0.57}_{-0.44}$	

state observed at this epoch is able to produce a high number of transitions in Fe XV-XVII in the 15-16 Å region. According to our model, absorption from the charges states OVI and OVII is also important in this source. These absorption lines are not easily recognisable, especially in Jan 2005 spectrum, due to the presence of the OVII emission line triplet. The OVI-OVII absorption is likely associated to the gas component at medium ionisation state.

The higher ionisation phase ( $\log \xi \sim 3$  ergs s cm $^{-1}$ ) is instead responsible for imprinting absorption at shorter wavelengths mainly in the Neon band around 12–14 Å. This component is characterised by a column density of the order of  $10^{22}$  cm $^{-2}$ , much higher than the one measured in the medium phase. In principle, warm gas at such ionisation level can produce absorption lines in the Fe K band around 6–7 keV, which may play a key role in shaping the Fe K alpha line profile (e.g. Reeves et al. 2004, Turner & Miller, 2009). Indeed, Longinotti et al. (2004) and Petrucci et al. (2007) reported a peculiar behaviour of the Fe K $\alpha$  line in their previous analysis of Mrk 841, but none of these works included a detailed modeling of the warm absorber. The detection of a high ionisation warm absorber in the RGS data prompted us to test for absorption effects on the Fe K line. This check was performed by simply applying our best fit model to the EPIC-pn data of Jan 2005, i.e. the spectrum with the highest column density in the high ionisation phase (Table 2). With the parameters frozen to the values of Table 2, we found that this warm absorber component is not sufficiently deep for introducing any additional curvature around the Fe line, neither for modifying the line profile itself.

#### 4.2. Density of the warm absorber

In about four-years time, the low-energy flux of Mrk 841 decreased by a factor of 3.5 (Table 1). In Jan 2005, when the source is fainter, we measure also a lower ionisation parameter for the cold phase, while the column density stays constant within the errors (Table 2). Given the uncertainty on the outflow velocity, we assume here that we detect the same gas material both in 2001 and 2005, albeit with different ionisation.

We estimated a lower limit for the density of such gas, assuming a recombination time of 1422 days (4 years time in between Jan 2001 and Jan 2005), i.e.  $t_s = \frac{t_o}{1+z}$  in the source rest frame. We considered all the Fe ions detected in the spectrum. Each ion has its own recombination time, which is inversely related to the gas density  $n_e$ , as reported in Bottorff et al. (2000) and Detmers et al. (2008):

$$t(X_i) = \left( \alpha_r(X_i) n_e \left[ \frac{f(X_{i+1})}{f(X_i)} - \frac{\alpha_r(X_{i-1})}{\alpha_r(X_i)} \right] \right)^{-1}$$

where  $t(X_i)$  is the recombination timescale of the ion  $X_i$ ,  $\alpha(X_i)$  is the recombination rate from ion  $X_{i-1}$  to ion  $X_i$  and  $f(X_i)$  represents the fraction of the element  $X$  at the ionization state  $i$ .

This relation allows us to put further constraint on the lower limit of the density. We used the values predicted by the best-fit global modelling of the absorber, as the quality of the data does not allow to perform a line-by-line fitting on the Fe ions, especially in the crowded region of the iron UTA. The associated error on the ionic column densities is therefore the scaled value of the error on the total  $N_H$ .

The gas density is a function of the recombination rates which are in turn a function of the gas temperature  $T_e$ , before recombination (Bottorff et al. 2000, Detmers et al. 2008). The value of  $T_e$  is linked to the ionisation parameter  $\xi$  via the ion-



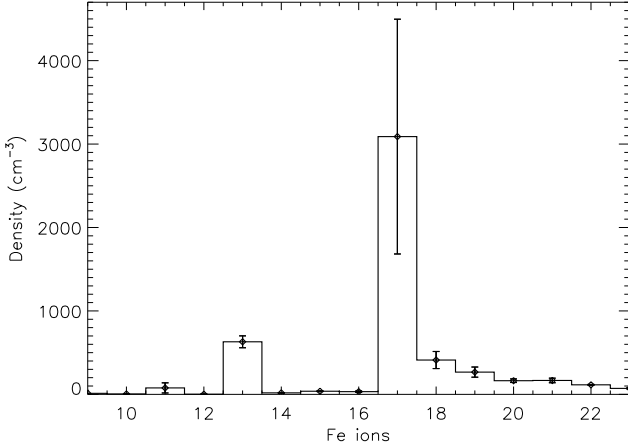


**Fig. 5.** Electron density in the warm absorber estimated using the recombination of the iron ions produced by the gas with  $\log \xi = 2.2 \pm 0.23$  and  $N_{\text{H}} \sim 1.2 \pm 0.5 \times 10^{21} \text{ cm}^{-2}$ .

isation balance. The error on  $\xi$  (Table 2), rather than the error on individual ionic column densities, has the major weight in the density determination. The radiative recombination rates for iron have been analytically determined using the expression and recombination coefficient provided in Woods et al. (1981).

In Fig. 5 we show the density lower limits for the Fe ions. The ion which provides the larger value for  $n = 3.1 \pm 1.4 \times 10^3 \text{ cm}^{-3}$  is Fe xvii.

#### 4.3. On the origin of the narrow emission lines and Radiative Recombination Continua

The following discussion is based chiefly on the findings for Jan 2005 spectrum, where the emission lines component is detected with highest significance. The narrowness of the RRC profiles is consistent with an electron temperature of  $\text{few} \times 10^4 \text{ K}$  and it seems to indicate that photoionisation from the central source is the primary mechanism acting on the surrounding gas (e.g. Kinkhabwala et al. 2002, Armentrout et al. 2007).

The relative intensity of line triplets in He-like ions provides an excellent diagnostic of the physical properties of the emitting plasma (Porquet & Dubau, 2000 and reference therein). In general, it has been observed that photoionisation processes in Seyfert Galaxies give rise to line triplets dominated by the forbidden transition (e.g. NGC 1068, Kinkhabwala et al. 2002). If we consider the line fluxes of the OVII triplet in Mrk 841, we note that their ratio is not typical of photoionisation, the less prominent line being the forbidden transition, as evident also from Figure 4. The intercombination component at  $21.790 \text{ \AA}$  is as strong as the resonance one, if not higher: the presence of a bad pixel in between the  $r$  and  $i$  lines does not allow a precise reconstruction of the  $r$  emission line. On the contrary, we measure an upper limit for the forbidden component. Since this line is not affected by instrumental effects and it is generally expected to be dominant in AGN spectra, this measurement provides a stringent limit to be considered in the discussion of the line ratios.

The  $R$  ratio  $\frac{f}{i}$  provides a compelling probe of the gas density in photoionised plasma (see Porquet & Dubau, 2000). The low value of this ratio ( $R < 0.76$ ) in Mrk 841 points to emission from a gas at very high density, i.e.  $n_e \geq 10^{11} \text{ cm}^{-3}$ . This result

partly recalls the case of the Seyfert 1 Galaxy Mrk 335 that displayed a photoionised OVII triplet with a dominant  $i$  line during a particularly low flux state (Longinotti et al. 2008).

The  $G$  ratio  $\frac{f+i}{r}$  instead is often used as an estimator of the electron temperature in the gas. We can estimate an upper limit on the  $G$  ratio by taking into account the upper limits on the three components of the triplet (i.e. the upper error bars for the two lines for which they are available and the upper limit on the  $f$  line). In this way, the  $G$  ratio is estimated to be less than 1.8. This limit is somewhat intermediate between a pure collisional and a pure photoionisation dominated plasma (see Figure 7 in Porquet & Dubau, 2000), possibly indicating that mixed processes are at work. We note some discrepancy between the temperature of the recombining plasma inferred in this work by the hybrid plasma by the calculations reported in Porquet & Dubau (2000). However, as highlighted for Mrk 3 (Sako et al. 2000) and NGC 4151 (Armentrout et al. 2007), the intensity of resonance lines in He-like triplets could be enhanced by photo-excitation mechanisms induced by the AGN, which leads to a decrease of the observed  $G$  ratio (Godet et al. 2004). In principle, such effect could be tested in our data by accounting for microturbulence in the resonance line (see Armentrout et al. 2007), but we recall that the velocity dispersion was undetermined even for the warm absorber lines (less than  $20 \text{ km s}^{-1}$ , see Section 3.1), thus not easily determinable with the present instrumental resolution.

#### 4.4. One photoionisation region for the warm absorber and the warm mirror?

While certainly very interesting, the soft X-ray properties in Mrk 841 are not unique: several AGNs show features from ionised plasma both in absorption and emission (e.g. NGC 4151, (Armentrout et al. 2007, Kraemer et al. 2005); NGC 3783 (Behar et al. 2003)). For some cases, attempts are being made to ascribe the two processes to the same photoionised plasma (e.g. NGC 4051, Nucita et al. in prep.). The main unknown is the geometry of the circumnuclear gas, which should act as a “warm mirror” for scattering the emission lines and, at the same time, it should intercept the observer’s line of sight for producing warm absorber features.

For a large number of X-ray obscured Seyfert galaxies there are several indications that the X-ray photoionisation region where the bulk of soft X-ray line emission takes place, is spatially coincident with the optical Narrow Line Region (NLR) (see Bianchi et al. 2006 and Guainazzi & Bianchi 2007). Seyfert 1 objects, with unobscured X-ray spectra, offer instead a direct view of the continuum source and the surrounding high density gas giving rise to optical broad lines (i.e. the Broad Line Region (BLR)), therefore introducing more diversity in determining the distribution of the hot plasma. As an example, in the Seyfert 1 NGC 4051 (Pounds et al. 2004) and NGC 5548 (Kaastra et al. 2002, Detmers et al. 2008) the gas density inferred from the observed emission lines indicates an origin in the NLR, whereas in Mrk 335, the high density line-emitting gas ( $n_e = 10^{9-11} \text{ cm}^{-3}$ ) was located within the source BLR (Longinotti et al. 2008).

The present study of Mrk 841 with the detection of an important warm absorber component and photoionised emission lines, provides the opportunity to compare and, possibly, link their properties. The ionisation parameter of the photoionised gas  $\xi = \frac{L}{n_e R^2}$  depends on the plasma electron density, its radial

distance from the source of radiation and the ionising luminosity. An average luminosity of  $10^{45}$  ergs  $s^{-1}$  was estimated from the SED in Figure 1 by integrating the data of Jan 2001 and Jan 2005 over 1-1000 Rydberg.

In Section 4.2, we derived a lower limit for the density of the warm absorber ( $>10^3$  cm $^{-3}$ ), which can loosely constrain the distance to  $<$  few tens of pc. Nevertheless, this constraint can be refined by using the limit on the density inferred by the OVII triplet ( $n_e \geq 10^{11}$  cm $^{-3}$ ), under the assumption that the emission lines originate within a gas at the same ionisation state of the warm absorber gas. Our two-phase model for Jan 2005 yields  $\log \xi \sim 1.5$  and  $3.2$  ergs s cm $^{-1}$  (see Table 2). However, in the model of the gas with  $\log \xi \sim 3.2$  ergs s cm $^{-1}$  the column density of OIX is much larger than the one of OVII and OVIII, therefore such a highly ionised gas is unlikely to produce OVII emission. Assuming the ionisation parameter of the low phase, the radial distance  $R$  of the “warm emitter gas” is then constrained to less than  $1.6 \times 10^{16}$  cm.

The person who wishes to put this result in the context of the source, may consider that the optical BLR lies at a radius of about  $4.4 \times 10^{16}$  cm, as roughly estimated from the FWHM of 5500 km  $s^{-1}$  in the optical lines (Boroson & Green, 1992). Thus, the ionised gas seem to encompass the BLR, analogously to Mrk 335 (Longinotti et al. 2008). We checked the agreement of the optical FWHM and the width of the OVII line triplet by fitting the three components with a Gaussian profile and freezing the rest of the model. We found the following FWHM for  $r$ ,  $i$ ,  $f$  respectively:  $400 \pm 60$ ,  $<1400$  and  $<5300$  km  $s^{-1}$ . While the velocities in the  $i$  and  $f$  components can still be reconciled with BLR, it is hard to explain the apparent inconsistency of the resonant line with the rest of the triplet. We remark however that the reconstruction of the  $r$  line is rather complex, as highlighted in Section 3.2.1. A more sophisticated modelling of the emission lines in high signal-to-noise data would be needed to supplement our hypothesis.

Few words must be spent on the line fluxes in the other two data sets for which only upper limits are available. The apparent lack of strong emission lines in Jan 2001 and Jan 2005 can be phenomenologically explained as an effect of the increased continuum flux. As a consequence, the emission component is swamped and covered in the observed spectra. While it is hard to exclude intrinsic variability in the emission line fluxes, especially since the continuum flux varies, there is no compelling evidence for variation in the present data.

#### 4.5. The broad OVII line in the RGS data

The broad emission line around  $\sim 21.7$  Å is detected with high significance in both 2005 observations. If fitted with a Gaussian profile, the FWHM corresponds to  $\sim 8200_{-4700}^{+7200}$  km  $s^{-1}$ , for Jan 2005. Considering the large error bars, this velocity is consistent with the optical H $\beta$  FWHM of 5500 km  $s^{-1}$  reported by Boroson & Green (1992). The presence of broad emission features in the soft X-ray spectra of Seyfert 1 Galaxies has been reported in the *Chandra*-LETG of Mrk 279 (Costantini et al. 2007), NGC 5548 (Steenbrugge et al. 2005), NGC 4051 (Steenbrugge et al. 2009), and in the *XMM-Newton*-RGS spectra of NGC 4051 (Ogle et al. 2004, Ponti et al. 2006). In most of these cases, the line profiles were consistent with Gaussians and in the first two sources, the velocity width of the emission lines was in agreement with measurements of UV lines in the BLR.

In the past, it was proposed to model RGS spectral lines from H-like ions in the Seyfert 1 Galaxies of MCG-6-30-15 and Mrk 766 with a relativistic profile (Branduardi-Raymont et al.

2001). We tried to convolve the OVII Gaussian emission line in Mrk 841 with a relativistic profile using the LAOR kernel (Laor, 1991) in the spectrum of Jan 2005. No good fit was found, perhaps not surprisingly since the data quality of Mrk 841 is not comparable to the long integration RGS spectra of the two bright sources mentioned above, making the test for relativistic broadening not viable in this source.

Considering the agreement of the OVII and H $\beta$  lines FWHM in Mrk 841, an BLR origin for the OVII broad line is favoured. Unfortunately, the lack of simultaneous UV spectral data for this source prevents us to perform a more detailed analysis of this feature and its relation to the multi-wavelength properties.

## 5. Summary of conclusions

In the following we summarise the main results of the first analysis of Mrk 841 high resolution X-ray spectra:

- Warm absorber: a two-phase warm absorber with  $\log \xi \sim 1.5$ – $2.2$  ergs s cm $^{-1}$  and  $\log \xi \sim 3$  ergs s cm $^{-1}$  is observed in the three spectra from 2001 through 2005; a moderate decrease in the ionisation state is observed going from the brightest flux state (2001) to the dimmer state (2005); no outflow is detected in the data; the high ionisation component has no effect in the Fe K band.
- Emission features: narrow OVII and NeIX emission lines are detected in Jan 2005 spectrum; the line ratio in the OVII triplet points to an origin in a gas at high electron density ( $n_e \geq 10^{11}$  cm $^{-3}$ ); the presence of narrow RRC from OVII and CVI is consistent with photoionisation processes; if it is assumed that the emission component and the warm absorber originate within a gas at the same ionisation state, the inferred distance for the emission lines is constrained within  $10^{16}$  cm from the central source.
- A broad Gaussian line centred at 21.7 Å is interpreted as emission from OVII. The FWHM is fully compatible with that of the optical broad emission lines in Mrk 841.

**Acknowledgements.** We thank the referee for providing useful comments on our work. This paper is based on observations obtained with the *XMM-Newton* satellite, an ESA science mission with instruments and contributions directly funded by ESA Member States and NASA. We acknowledge support from the Faculty of the European Space Astronomy Centre (ESAC) and from the French GDR PCHE for financially supporting the collaboration meetings necessary to finalise this work. GP thanks ANR for support (ANR-06-JCJC-0047).

## References

- Anders, E., & Grevesse, N. 1989, *Geochim. Cosmochim. Acta*, 53, 197  
 Arav, N., et al. 2007, *ApJ*, 658, 829  
 Armentrout, B. K., Kraemer, S. B., & Turner, T. J. 2007, *ApJ*, 665, 237  
 Behar, E., Sako, M., & Kahn, S. M. 2001, *ApJ*, 563, 497  
 Behar, E., Rasmussen, A. P., Blustin, A. J., Sako, M., Kahn, S. M., Kaastra, J. S., Branduardi-Raymont, G., & Steenbrugge, K. C. 2003, *ApJ*, 598, 232  
 Bianchi S., Matt G., Haardt F., Maraschi L., Nicastro F., Perola G. C., Petrucci P. O., Piro L., 2001, *A&A*, 376, 77  
 Bianchi S., Matt G., Balestra I., Guainazzi M., Perola G. C., 2004, *A&A*, 422, 65  
 Bianchi, S., Guainazzi, M., & Chiaberge, M. 2006, *A&A*, 448, 499  
 Blustin, A. J., Page, M. J., Fuerst, S. V., Branduardi-Raymont, G., & Ashton, C. E. 2005, *A&A*, 431, 111  
 Boroson, T. A., & Green, R. F. 1992, *ApJS*, 80, 109  
 Bottorff, M. C., Korista, K. T., & Shlosman, I. 2000, *ApJ*, 537, 134  
 Branduardi-Raymont, G., Sako, M., Kahn, S. M., Brinkman, A. C., Kaastra, J. S., & Page, M. J. *A&A*, 365, L140  
 Cash, W. 1979, *ApJ*, 228, 939  
 Costantini, E., et al. 2007, *A&A*, 461, 121  
 Crenshaw, D. M., Kraemer, S. B., & George, I. M. 2003, *ARA&A*, 41, 117  
 Crummy, J., Fabian, A. C., Gallo, L., & Ross, R. R. 2006, *MNRAS*, 365, 1067



- den Herder, J. W., et al. 2001, *A&A*, 365, L7
- Detmers, R. G., Kaastra, J. S., Costantini, E., McHardy, I. M., & Verbunt, F. 2008, *A&A*, 488, 67
- Dickey, J. M., & Lockman, F. J. 1990, *ARA&A*, 28, 215
- Ferland, G. J., Korista, K. T., Verner, D. A., Ferguson, J. W., Kingdon, J. B., & Verner, E. M. 1998, *PASP*, 110, 761
- Gabel, J. R., et al. 2005, *ApJ*, 631, 741
- George I. M., Nandra K., Fabian A. C., Turner T. J., Done C., Day C. S. R., 1993, *MNRAS*, 260, 111
- Gierliński, M., & Done, C. 2004, *MNRAS*, 349, L7
- Godet, O., Collin, S., & Dumont, A.-M. 2004, *A&A*, 426, 767
- Guainazzi, M., & Bianchi, S. 2007, *MNRAS*, 374, 1290
- Kaastra, J. S., Mewe, R., & Nieuwenhuijzen, H. 1996, *UV and X-ray Spectroscopy of Astrophysical and Laboratory Plasmas*, 411
- Kaastra, J. S., Steenbrugge, K. C., Raassen, A. J. J., van der Meer, R. L. J., Brinkman, A. C., Liedahl, D. A., Behar, E., & de Rosa, A. 2002, *A&A*, 386, 427
- Kaspi, S., et al. 2001, *ApJ*, 554, 216
- Kinkhabwala, A., et al. 2002, *ApJ*, 575, 732
- Kraemer, S. B., et al. 2005, *ApJ*, 633, 693
- Krongold, Y., Nicastro, F., Brickhouse, N. S., Elvis, M., & Mathur, S. 2005, *ApJ*, 622, 842
- Krongold, Y., Nicastro, F., Elvis, M., Brickhouse, N., Binette, L., Mathur, S., & Jiménez-Bailón, E. 2007, *ApJ*, 659, 1022
- Laor A., 1991, *ApJ*, 376, 90
- Liedahl, D. A., & Paerels, F. 1996, *ApJ*, 468, L33
- Liedahl, D. A. 1999, *X-Ray Spectroscopy in Astrophysics*, 520, 189
- Longinotti, A. L., Nandra, K., Petrucci, P. O., & O'Neill, P. M. 2004, *MNRAS*, 355, 929
- Longinotti, A. L., Nucita, A., Santos-Lleo, M., & Guainazzi, M. 2008, *A&A*, 484, 311
- Nandra K., Turner T. J., George I. M., Fabian A. C., Shrader C., Sun W.-H., 1995, *MNRAS*, 273, 85
- Nandra K., George I. M., Mushotzky R. F., Turner T. J., Yaqoob T., 1997, *ApJ*, 477, 602
- Netzer, H., Chelouche, D., George, I. M., Turner, T. J., Crenshaw, D. M., Kraemer, S. B., & Nandra, K. 2002, *ApJ*, 571, 256
- Ogle, P. M., Mason, K. O., Page, M. J., Salvi, N. J., Cordova, F. A., McHardy, I. M., & Priedhorsky, W. C. 2004, *ApJ*, 606, 151
- Petrucci P. O., et al., 2002, *A&A*, 388, L5
- Petrucci, P. O., et al. 2007, *A&A*, 470, 889
- Ponti, G., Miniutti, G., Cappi, M., Maraschi, L., Fabian, A. C., & Iwasawa, K. 2006, *MNRAS*, 368, 903
- Porquet, D., & Dubau, J. 2000, *A&AS*, 143, 495
- Porquet, D., Mewe, R., Dubau, J., Raassen, A. J. J., & Kaastra, J. S. 2001, *A&A*, 376, 1113
- Pounds, K. A., Reeves, J. N., King, A. R., & Page, K. L. 2004, *MNRAS*, 350, 10
- Reeves, J. N., Nandra, K., George, I. M., Pounds, K. A., Turner, T. J., & Yaqoob, T. 2004, *ApJ*, 602, 648
- Reynolds, C. S. 1997, *MNRAS*, 286, 513
- Sako, M., Kahn, S. M., Paerels, F., & Liedahl, D. A. 2000, *ApJ*, 543, L115
- Sako, M., et al. 2001, *A&A*, 365, L168
- Steenbrugge, K. C., et al. 2005, *A&A*, 434, 569
- Steenbrugge, K. C., Fenovčík, M., Kaastra, J. S., Costantini, E., & Verbunt, F. 2009, *A&A*, 496, 107
- Véron-Cetty M.-P., Véron P., 2001, *A&A*, 374, 92
- Turner, T. J., & Miller, L. 2009, *A&A Rev.*, 17, 47
- Weaver K. A., Gelbord J., Yaqoob T., 2001, *ApJ*, 550, 261
- Woods, D. T., Shull, J. M., & Sarazin, C. L. 1981, *ApJ*, 249, 399